L-selectin shedding is activated specifically within transmigrating pseudopods of monocytes to regulate cell polarity in vitro

Karolina Rzeniewicz[a], Abigail Newe[a], Angela Rey Gallardo[a], Jessica Davies[a], Mark R. Holt[b], Ashish Patel[c], Guillaume T. Charras[d], Brian Stramer[b], Chris Molenaar[a], Thomas F. Tedder[e], Maddy Parsons[b], and Aleksandar Ivetic[a,1]

[a]Membrane/Cytoskeleton Signalling Group, Cardiovascular Division, King's College London, British Heart Foundation Centre of Research Excellence, London SE5 9NU, United Kingdom; [b]Randall Division of Cell and Molecular Biophysics, King's College London, London SE1 1UL, United Kingdom; [c]Cardiovascular Division, Academic Department of Surgery, King's College London, Biomedical Research Centre at Guy's & St. Thomas' National Health Service Foundation Trust and King's College London, London SE1 7EH, United Kingdom; [d]London Centre for Nanotechnology, London WC1H 0AH, United Kingdom; and [e]Department of Immunology, Duke University Medical Center, Durham, NC 27710

L-selectin is a cell adhesion molecule that tethers free-flowing leukocytes from the blood to luminal vessel walls, facilitating the initial stages of their emigration from the circulation toward an extravascular inflammatory insult. Following shear-resistant adhesion to the vessel wall, L-selectin has frequently been reported to be rapidly cleaved from the plasma membrane (known as ectodomain shedding), with little knowledge of the timing or functional consequence of this event. Using advanced imaging techniques, we observe L-selectin shedding occurring exclusively as primary human monocytes actively engage in transendothelial migration (TEM). Moreover, the shedding was localized to transmigrating pseudopods within the subendothelial space. By capturing monocytes in midtransmigration, we could monitor the subcellular distribution of L-selectin and better understand how ectodomain shedding might contribute to TEM. Mechanistically, L-selectin loses association with calmodulin (CaM; a negative regulator of shedding) specifically within transmigrating pseudopods. In contrast, L-selectin/CaM interaction remained intact in nontransmigrated regions of monocytes. We show phosphorylation of L-selectin at Ser 364 is critical for CaM dissociation, which is also restricted to the transmigrating pseudopod. Pharmacological or genetic inhibition of L-selectin shedding significantly increased pseudopodial extensions in transmigrating monocytes, which potentiated invasive behavior during TEM and prevented the establishment of front/back polarity for directional migration persistence once TEM was complete. We conclude that L-selectin shedding directly regulates polarity in transmigrated monocytes, which affirms an active role for this molecule in driving later stages of the multistep adhesion cascade.

calmodulin | invasion | leukocyte | migration | biglycan

The passage of leukocytes from the circulation toward the surrounding extravascular space is a critical event in the inflammatory response (1–3). The multistep adhesion cascade defines the increasingly adhesive steps leukocytes make with the endothelium to exit the circulation and enter the surrounding microenvironment (4). Each step of the cascade [tethering, rolling, slow rolling, firm adhesion, and transendothelial migration (TEM)] critically depends on cell adhesion molecules expressed on both leukocytes and endothelial cells. Such cell adhesion molecules have been identified and characterized to act in a sequential and interdependent manner. The molecular mechanism driving leukocyte integrin function during the multistep adhesion cascade is relatively well defined (4–6). In contrast, mechanisms underpinning the regulation of nonintegrin receptors are only beginning to emerge. One such example, L-selectin, is known to promote the initial tethering and subsequent rolling of leukocytes along activated endothelial cells (7). Knocking out L-selectin in mice has provided compelling evidence for this cell adhesion molecule in directing neutrophils

toward sites of inflammation (8). Intriguingly, knocking out L-selectin has a dramatic impact on neutrophil chemotaxis in vivo, but the molecular basis for this observation remains elusive (9). Following firm adhesion, L-selectin is broadly considered to be proteolytically cleaved (or shed) at a defined extracellular membrane/proximal domain by membrane-associated matrix metalloproteinases (10). The best-characterized "sheddase" is a disintegrin and metalloproteinase (ADAM17; or TNF-α concerting enzyme) (11). Shedding of L-selectin hinges on its interaction with calmodulin (CaM); binding of CaM to L-selectin protects from shedding, and leukocyte activation leads to CaM dissociation from the L-selectin tail to drive shedding (12). What promotes CaM dissociation is not known, but mutating the L-selectin tail can have a profound impact on the shedding response (13–15). L-selectin shedding is a rapid event, and the biological significance of its outcome may be numerous (10). In respect to leukocyte recruitment, L-selectin shedding would rapidly halt any further contribution of this molecule toward cell adhesion, signaling, or migration. The timing of L-selectin shedding is therefore critical in relation to input signals derived from other surface receptors contributing to the same cellular event (7). Our understanding of coordinated receptor signaling during TEM is extremely poor,

---

Significance

During an inflammatory response, L-selectin, an immune cell-specific adhesion molecule, guides monocytes from the bloodstream toward the surrounding extravascular environment (termed "transmigration"). We show, under conditions that mimic blood flow, that L-selectin is proteolytically cleaved (or shed) exclusively within leading migratory fronts (pseudopods) of actively transmigrating monocytes. Calmodulin/L-selectin interaction, which acts to block shedding, is lost through Ser phosphorylation of the L-selectin cytoplasmic tail, occurring specifically within transmigrating pseudopods. Blocking L-selectin shedding specifically during transmigration increases pseudopod numbers, leading to defective front/back polarity that is essential for migration. These findings are the first to report, to our knowledge, an extended role for L-selectin in regulating morphological changes in leukocytes that are required for migration.

---

mainly because insight into the molecular regulation of each individual cell adhesion molecule is still lacking.

The contribution of L-selectin to the multistep adhesion cascade has been defined through two major experimental approaches: function-blocking studies (using soluble ligand or monoclonal antibody) and gene KO/knock-in mice. Such studies have built the foundation of our knowledge of the adhesion cascade. However, these approaches limit our understanding of where the targeted molecule's first nonredundant step is required. Direct imaging of cell adhesion molecules in space and time, during recruitment under flow conditions, can provide additional clues beyond the first nonredundant point of execution. Here, we have used a series of advanced imaging techniques to pinpoint where and when L-selectin is cleaved during the multistep adhesion cascade. Using primary human monocytes, we reveal the shedding event was occurring specifically during TEM and not before. Through stable expression of WT and mutant forms of L-selectin tagged to GFP or red fluorescent protein (RFP), we could define the shedding event on a mechanistic level in THP-1 cells. Fluorescence lifetime imaging microscopy (FLIM) enabled quantitative measurement of the fluorescence resonance energy transfer (FRET) efficiency between L-selectin–GFP and CaM-RFP, allowing us to monitor the subcellular distribution of their interaction during TEM. We show, for the first time to our knowledge, that L-selectin shedding can regulate the invasive behavior of monocytes crossing activated endothelial monolayers under flow. Furthermore, we show that polarity in transmigrated monocytes is disrupted if shedding of L-selectin is blocked. Taken together, these results reveal previously unidentified roles for L-selectin that extend beyond tethering and rolling.

Results

Polarized Shedding of L-Selectin Occurs in Primary Human Monocytes Undergoing TEM.
To determine the spatiotemporal distribution of L-selectin during TEM, primary human monocytes were labeled with leukocyte adhesion molecule-1 14 (LAM1-14) monoclonal antibody directly conjugated to Alexa Fluor 555. LAM1-14 is a non–function-blocking monoclonal antibody that recognizes the extracellular EGF-like domain of L-selectin, but not its C-type lectin domain (16). Monocytes were perfused over TNF-activated human umbilical vein endothelial cells (HUVECs), and L-selectin expression was monitored in real-time by fluorescence time-lapse microscopy. From the point of capture to activated endothelial cells, monocytes completed TEM at an average time of 5 min (Fig. 1 A and B) and lost L-selectin expression exclusively during TEM, but not before (Fig. 1C and Movie S1). Transmigration under static conditions took 8 min (Fig. S1A), with the extra time dedicated to more crawling before TEM. To verify that LAM1-14 antibody did not interfere with L-selectin expression during TEM, unlabeled monocytes were perfused under similar conditions, and were subsequently fixed, permeabilized, and stained for F-actin and L-selectin. Confocal microscopy revealed that all of the monocytes arrested on the apical surface of the endothelium were L-selectin–positive but all fully transmigrated cells were L-selectin–negative. This observation was reversed if the monocytes were pretreated with 10 μM sheddase inhibitor, TNF-α protease inhibitor-0 (TAPI-0) (Fig. 1 D and E). To investigate where and when L-selectin shedding was occurring in more detail, primary monocytes were perfused over TNF-activated HUVECs for shorter periods (3–6 min) and immediately fixed and stained with phalloidin, anti–vascular endothelial (VE)-cadherin, and LAM1-14 antibody. In all cases, L-selectin expression was detected in monocyte pseudopods protruding beneath the endothelial monolayer (Fig. 1F, Fig. S1B, and Movie S2). These results strongly suggest that the loss of L-selectin expression is occurring specifically within pseudopods protruding beneath the endothelial monolayer and not before. Moreover, they imply that

L-selectin may actively participate in steps of the adhesion cascade that extend beyond tethering and rolling.

Generation of THP-1 Monocyte Cell Line Stably Expressing L-Selectin–GFP.
To interrogate the molecular basis of our observations, we generated monocyte-derived THP-1 cells stably expressing WT L-selectin–GFP (Fig. S2A). THP-1 cells do not express endogenous L-selectin, providing a clean background in which to study L-selectin–GFP. Transduced cell lines were subjected to rigorous cell biological and biochemical characterization to ensure that C-terminal tagging of L-selectin to GFP did not interfere with function. SEM demonstrated that, irrespective of L-selectin–GFP expression, THP-1 cells presented abundant microvilli under resting conditions (Fig. S2B). Immunogold labeling of L-selectin showed that the majority of L-selectin was enriched on microvilli (Fig. S2B), as has been shown previously for endogenous L-selectin on numerous primary leukocytes (17). Endogenous CaM was coprecipitated with L-selectin–GFP from whole-cell lysates, demonstrating interaction with known binding partners (Fig. S2C, lane 2). The ezrin-radixin-moesin (ERM) family members ezrin and moesin are known binding partners of L-selectin (18, 19). Coexpression of L-selectin–RFP with either N-terminal moesin-GFP or ezrin-GFP led to detectable FRET measured by FLIM (Materials and Methods and Fig. S2D), again suggesting the tag was noninterfering. Perfusion of L-selectin–GFP–positive THP-1 cells over a series of increasing sialyl Lewis X (sLe^x; a known ligand for L-selectin) densities led to dose-dependent decreases in rolling velocity and concomitant increases in rolling flux (Fig. S2E). In keeping with a previous study that used U937 cells (20), increased recruitment to TNF-activated HUVECs was observed in THP-1 cells expressing L-selectin–GFP under flow conditions, but not in cells expressing equivalent levels of GFP alone (Fig. S2F). Confocal microscopy revealed THP-1 cells undergoing bona fide TEM, breaching VE-cadherin–positive junctions and transmigrating beneath the HUVEC monolayer (Fig. S2G). Note that THP-1 cells are too large to undergo full TEM, which makes them an excellent model for studying the molecular events regulating TEM. Treatment of THP-1 cells with phorbol ester (Fig. S2H) or coculture with TNF-activated HUVEC monolayers (Fig. S2I) led to robust L-selectin shedding, as judged by Western blotting of the GFP tag. Taken together, these data show that L-selectin–GFP behaves as expected for untagged L-selectin, and thus provides a suitable model for interrogating the molecular events driving the shedding response during TEM.

WT L-Selectin–GFP Is Organized into Clusters Within Transmigrating Pseudopods.
Analysis of primary human monocytes showed L-selectin shedding occurred only in cells undergoing TEM (Fig. 1). To probe this finding in more detail, THP-1 cells expressing WT L-selectin-GFP or GFP alone were fixed in 4% [(vol/vol) in PBS] paraformaldehyde (PFA) following 6 min or 15 min of perfusion over TNF-activated HUVECs to reflect early and later phases of TEM. As time progressed, WT L-selectin appeared to be organized into GFP-positive "spots" within pseudopods protruding beneath the endothelial monolayer. The number of L-selectin–GFP spots increased over time, and they were located specifically in the transmigrated pseudopods, which did not appear in cells expressing GFP alone (Fig. 2 A–C). These spots were reminiscent of the L-selectin clusters seen in pseudopods protruding beneath the endothelium in primary monocytes (Fig. 1F and Fig. S1B). To quantify the extent of L-selectin clustering in THP-1 cells undergoing TEM, L-selectin–RFP was introduced into THP-1 cells expressing L-selectin–GFP and clustering was analyzed in transmigrating cells by FRET/FLIM. A significantly higher degree of L-selectin clustering was seen in transmigrated pseudopods compared with the area of the monocyte that remained above the endothelium (Fig. 2D). To determine if the GFP spots were full-length or cleaved forms of L-selectin, THP-1
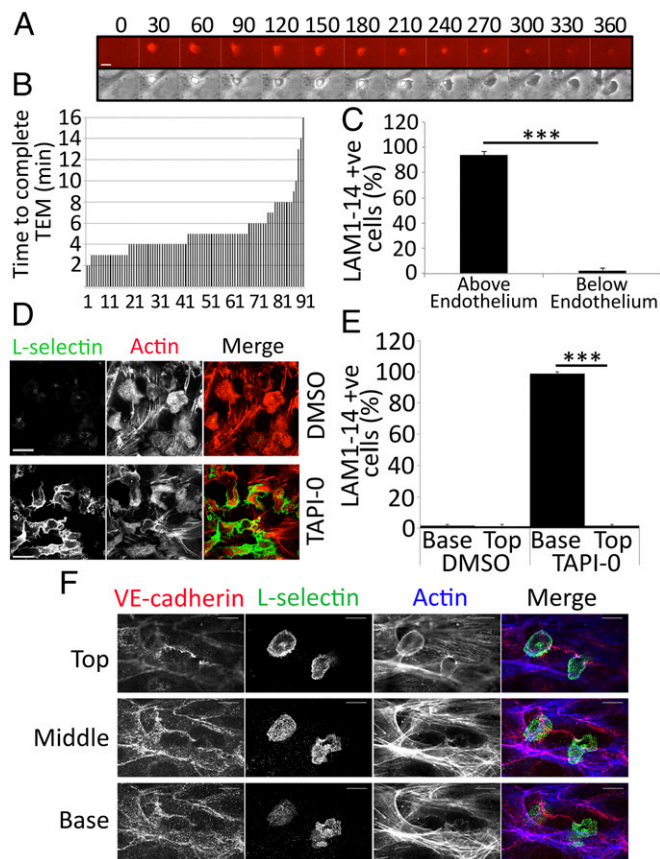
Fig. 1. Shedding of L-selectin occurs specifically during TEM. (*A*) Image series of a primary monocyte, prelabeled with Alexa Fluor 555-conjugated LAM1-14, undergoing TEM. Each frame is taken every 30 s. (*Upper*) LAM1-14 signal (Alexa Fluor 555 channel) in this image series, showing the subcellular distribution of L-selectin. (*Lower*) Phase contrast image series. (Scale bar: 5 μm.) The time code is written above every frame in seconds (Movie S1). (*B*) Primary monocytes were continually perfused over TNF-activated HUVECs and recorded at four frames per minute under phase contrast (10× objective lens) with an inverted Olympus IX-81 digital time-lapse microscope. To avoid bias, three fields of view were selected before monocyte perfusion. The rate of TEM was expressed as the time taken from initial binding from flow to complete TEM (as shown in *A*). The total number of cells scored was 93. Measurements were taken from three independent flow experiments and from three different healthy donors. (*C*) Primary monocytes prelabeled with LAM1-14 were perfused over TNF-activated HUVECs and recorded by time-lapse fluorescence microscopy for 25 min. At the halfway point of each flow assay, monocytes were scored as being either above or below the endothelium based on their phase contrast, and were subsequently measured as a percentage of cells expressing L-selectin within these specified compartments (Movie S1). Data were acquired from an average of three independent experiments using at least three fields of view for each assay. A two-tailed, unpaired Student's *t* test was used for statistical analysis. ***P < 0.001. (*D*) Unlabeled primary monocytes were perfused over TNF-activated HUVECs for 15 min, followed by 10 min of perfusion with media alone to promote >95% TEM. The glass coverslip (containing HUVECs and adhered/transmigrated monocytes) was subsequently detached from the flow chamber and immediately fixed in 4% (vol/vol) PFA. Specimens were stained with TRITC-phalloidin (to visualize F-actin) and LAM1-14 (to visualize L-selectin), followed by Alexa 488-conjugated secondary antibody. All images were acquired by confocal microscopy (63× objective lens) at the basolateral aspect of the HUVEC monolayer, capturing only transmigrated monocytes. (*Upper*) Images represent carrier (DMSO)-treated cells. (*Lower*) Images are 10 μM TAPI-0–treated cells. (Scale bars: 16.5 μm.) (*E*) Flow assays performed in *D* were scored as the percentage of L-selectin–positive monocytes above ("Top") or below ("Base") the endothelium, treated with DMSO or 10 μM TAPI-0. (*F*) Unlabeled monocytes were captured in midtransmigration by fixing specimens in 4% (vol/vol) PFA after 6 min of perfusion over TNF-activated HUVECs. (Top, Middle, and Base) Each optical

section reveals the subcellular distribution of VE-cadherin (Alexa Fluor 548), L-selectin (Alexa Fluor 488), and F-actin (phalloidin-Alexa Fluor 633). This image is cropped from a broader field of view, which can be seen in Fig. S1*B*. The image represents one monocyte undergoing TEM and another adhered to the apical aspect of the endothelium. Note that the continuity of VE-cadherin staining is breached at the point of transmigration, which is a hallmark feature of transmigration, and L-selectin is clearly expressed in the transmigrated pseudopod. (Scale bars: 10 μm.)

cells expressing only L-selectin–GFP were perfused and fixed as before, and subsequently counterstained with LAM1-14 antibody. The degree of colocalization between the GFP (intracellular) and LAM1-14 (extracellular) signals was used to measure the extent of L-selectin shedding in THP-1 cells undergoing TEM (Fig. 2*E*). Using Manders' colocalization coefficiency (21), above and below the endothelium, revealed a significant decrease in the degree of overlap specifically within the transmigrated part of the cell (Fig. 2*F*).

Cells expressing a deletion mutant of L-selectin–GFP called ΔM-N, which resist shedding in response to cell activation (22), were used to monitor differences in subcellular distribution with WT L-selectin–GFP. First, as predicted, no change in the colocalization between LAM-1 and GFP signals was seen in transmigrating THP-1 cells expressing ΔM-N L-selectin–GFP (Fig. S3). Interestingly, the number of GFP-positive spots within transmigrating pseudopods increased over time in cells expressing WT, but not ΔM-N L-selectin (Fig. 2*G*). Taken together, this observation would suggest that WT L-selectin is potentially corralled into spots before it is cleaved. Spinning disk confocal microscopy also confirmed in real time that these spots appeared only in the WT cells undergoing TEM under flow conditions (Movie S3).

Subendothelial Glycans Promote Clustering of L-Selectin. In addition to binding sLe[x], L-selectin can bind to chondroitin, dermatan, and heparan sulfate proteoglycans (HSPGs) (23–26). The recent identification of an increasing HSPG gradient toward the basolateral aspect of endothelial cells (27) led us to explore whether biglycan, a known ligand for L-selectin (25), was expressed in HUVECs. Western blotting and confocal imaging confirmed this to be the case. Moreover, protein levels did not change following TNF stimulation (Fig. 2 *H* and *I* and Fig. S4*A*). In keeping with previous findings (27), confocal imaging of extracellular biglycan was expressed in higher densities in the basolateral aspect of the endothelium (Fig. S4*B*). THP-1 cells expressing L-selectin–GFP/RFP enabled direct quantitation of clustering on purified immobilized biglycan through FRET/FLIM analysis. A significant dose-dependent increase in clustering of WT L-selectin, but not ΔM-N L-selectin, was observed under these conditions (Fig. 2*J*), further supporting the concept that subendothelial glycans can cluster L-selectin.

Monitoring CaM/L-Selectin Interaction in Monocytes During TEM Under Flow. The shedding of L-selectin hinges on its interaction with CaM (12). To address the molecular mechanism driving L-selectin shedding, THP-1 cells expressing WT L-selectin–GFP were stably transduced with CaM-RFP and perfused over TNF-activated HUVECs for 6 min, followed by continued perfusion with medium for a further 19 min. These times correspond to periods of minimum and maximum shedding, respectively (as estimated from Fig. S2*I*). Cells were then fixed and analyzed by FRET/FLIM. After 6 min, FRET between CaM and L-selectin was equal in both the nontransmigrated and transmigrated parts of the cell, suggesting that L-selectin is protected from shedding at this stage (Fig. 3*A*). By 25 min, FRET between CaM-RFP and L-selectin–GFP was significantly reduced in transmigrated pseudopods (Fig. 3*B*). In agreement with visualizing polarized
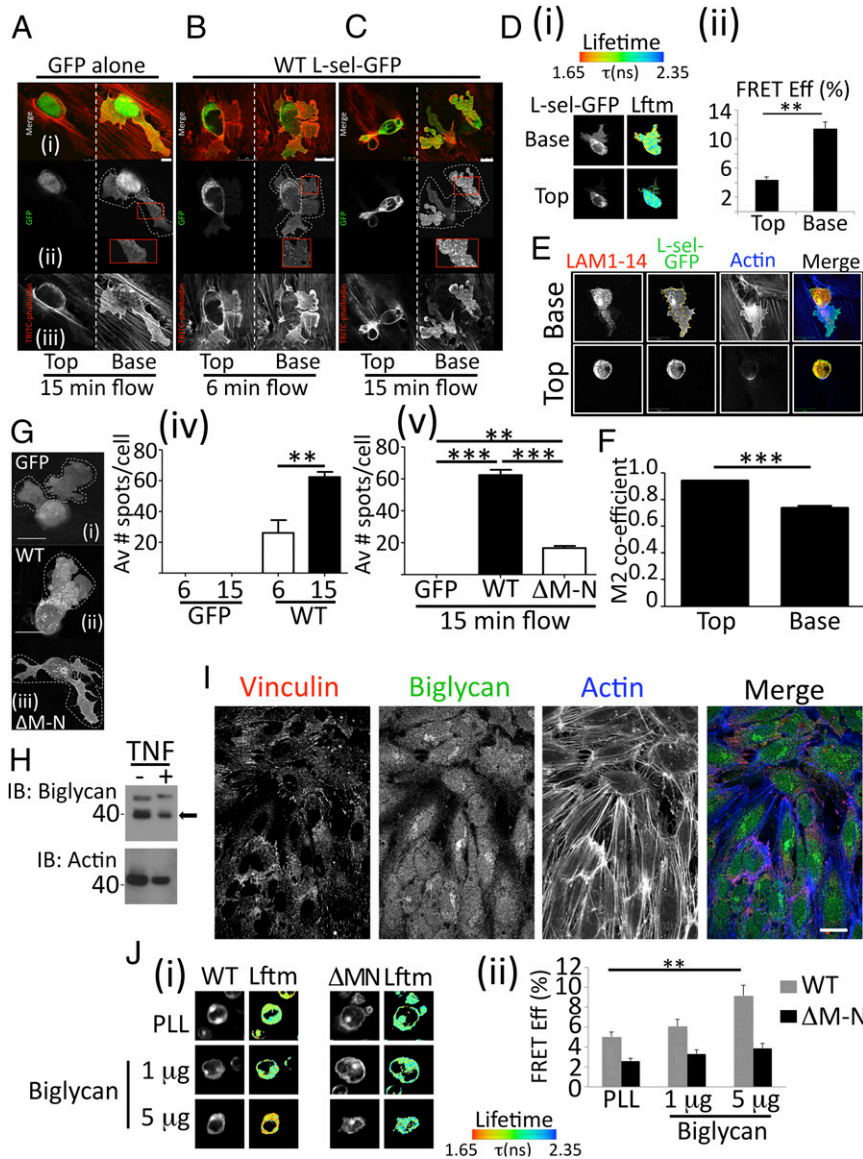
Fig. 2. Clustering of L-selectin by subendothelial glycans. (*A–C*) Cells expressing either GFP alone or WT L-selectin (L-sel)–GFP were perfused over TNF-activated HUVECs for 6 min or 15–20 min (referred to as "15 min" in figure), and subsequently fixed in 4% (vol/vol) PFA and stained with TRITC-phalloidin. The horizontal panel of images represents (*i*) merge of channels, (*ii*) GFP signal, and (*iii*) phalloidin signal. Optical slices are taken for each transmigrating cell above (*Left*, Top vertical panel) and below (*Right*, Base vertical panel) the endothelial monolayer. Dotted lines surrounding each cell in the GFP channel indicate pseudopodial extensions protruding beneath the endothelial monolayer. (*Insets*) Example of GFP-positive "spots" that appear exclusively in THP-1 cells expressing WT L-selectin–GFP, which increase in number over time (compare *Insets* between 6 and 15 min of flow). [Scale bars (in merge panels): *A*, 5 μm; *B* and *C*, 10 μm.] (*D*, *i*) FRET/FLIM analysis of transmigrating THP-1 cells coexpressing L-selectin–GFP/RFP. Cells were perfused over TNF-activated HUVECs for 15–20 min, fixed, and prepared for FRET/FLIM analysis (*Materials and Methods*). The lifetime of fluorescence (Lftm) is expressed as a pseudocolor scale from red (low lifetime with a very high probability of interaction) to blue (high lifetime with a very low probability of interaction). (*D*, *ii*) Error bars represent SEM. A two-tailed unpaired Student's *t* test was used for statistical analysis. **$P < 0.001$. A total of 22 cells were analyzed. Eff, efficiency. (*E*) THP-1 cells expressing WT L-selectin–GFP were perfused over TNF-activated HUVECs for 15 min, fixed in PFA, and stained for LAM1-14 Alexa Fluor 555 and phalloidin conjugated to Alexa Fluor 633. (Scale bar: 14 μm.) (*F*) Manders' colocalization coefficient (M2) specifically refers to the fraction of LAM1-14 signal colocalizing with the GFP signal. Analysis was performed on at least 15 cells using Volocity cellular imaging and analysis software (version 6.0). A two-tailed unpaired Student's *t* test was used to calculate differences between Top and Base. Data are expressed as SEM. ***$P < 0.0002$. (*G*) GFP-positive spots counted in transmigrating pseudopods of THP-1 cells expressing (*i*) GFP alone, (*ii*) WT L-selectin–GFP, or (*iii*) ΔM-N L-selectin-GFP. (Scale bar: 10 μm.) GFP spots were counted in pseudopods of GFP alone or in WT L-selectin–GFP cells (*iv*) following 6 or 15 min of continuous perfusion or (*v*) in all three cell lines after 15 min of continuous perfusion. **$P < 0.001$; ***$P = 0.0002$. Av, average. (*H*) HUVEC monolayers were stimulated with or without TNF. Western blotting detects biglycan before and after TNF expression (an arrow marks the position of biglycan). The actin loading control below shows no change in biglycan expression after TNF stimulation ($n = 5$; analysis shown in Fig. S4). IB, immunoblot. (*I*) Confocal imaging of the basolateral aspect of the HUVEC monolayer stimulated with TNF. Vinculin staining identifies focal adhesions, which are located in the basolateral aspect of the HUVEC monolayer. Actin cables (highlighted by Alexa Fluor 633 staining) are a characteristic feature of TNF-activated HUVECs. Biglycan staining (identified with Alexa Fluor 488 secondary antibody) is clearly located at the basolateral aspect of activated HUVEC monolayers. (Scale bar: 25 μm.) (*J*) THP-1 cells expressing L-selectin–GFP/RFP were plated onto (*i*) poly-L-lysine (PLL) or increasing biglycan concentrations, and (*ii*) FRET between the fluorescent probes was measured by FLIM. A two-tailed unpaired Student's *t* test and SEM are represented in error bars. **$P = 0.001$. The Lftm is expressed as a pseudocolor scale from red (low lifetime with a very high probability of interaction) to blue (high lifetime with a very low probability of interaction).
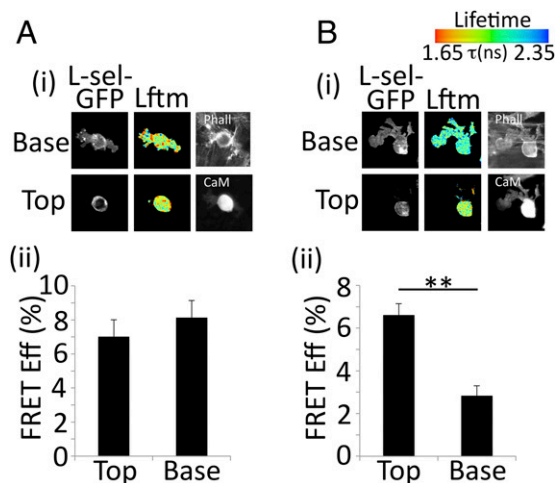
Fig. 3. CaM/L-selectin interaction is lost specifically within transmigrating monocyte pseudopods. THP-1 cells coexpressing WT L-selectin–GFP and CaM-RFP were perfused over TNF-activated HUVECs for either 6 (*A*) or 25 (*B*) min, fixed in PFA, and prepared for FRET/FLIM analysis. All 25-min flow assays were perfused with THP-1 cells for the first 6 min, followed by 19 min of flow with media alone. This procedure ensured that analysis represented perfusion for a minimum of 15 min of binding and transmigration across HUVECs. (*i*) Representative lifetime images, alongside single fluorescence channels for L-selectin–GFP, CaM-RFP, and phalloidin Alexa Fluor 633 channels. Note that CaM-RFP was acquired by wide-field fluorescence, because there was no capacity for confocal imaging on this channel. (*ii*) FRET efficiencyperformed on at least 15 cells for each time point. A two-tailed unpaired Student's *t* test was used to calculate differences between Top and Base, and error bars represent SEM. *******P* < 0.01. Lftm is expressed as a pseudocolor scale from red (low lifetime with a very high probability of interaction) to blue (high lifetime with a very low probability of interaction).

shedding in primary monocytes (Fig. 1 and Movie S1), CaM/L-selectin interaction occurs in a polarized manner and its loss is restricted to the transmigrated part of the THP-1 cell.

L-Selectin S364 Regulates CaM Binding and Shedding in Monocytes. Human L-selectin possesses two Ser residues that can be phosphorylated following cell activation (28). Mouse L-selectin and human L-selectin possess a conserved Ser residue at position 364, which hints at mechanistically conserved pathways regulating shedding and possibly CaM binding (Fig. 4*A*). To test whether S364 phosphorylation regulated CaM binding in vitro, a fixed concentration of purified recombinant CaM was incubated with a range of peptide concentrations corresponding to the 17-aa tail of L-selectin, phosphorylated at one or both Ser residues. Disuccinimidyl suberate cross-linking of CaM/peptide complexes was detected on polyacrylamide gels as an electrophoretic mobility shift (Fig. 4*B*, arrowhead). Densitometric analysis of the retarded CaM/peptide complex revealed that binding was highest with either nonphosphorylated or phospho-S367 peptides. In contrast, phosphorylation at S364 blocked CaM binding almost completely (Fig. 4 *B* and *C*). Phosphorylation at both Ser residues also blocked CaM binding, suggesting a dominant role for S364 in this process.

To determine if similar interactions exist in intact monocytes, THP-1 cells were engineered to stably express CaM-RFP and L-selectin–GFP S364 or S367 Ala or Asp mutations to block or mimic phosphorylation, respectively. Cells were perfused over TNF-activated HUVECs, and FRET between L-selectin and CaM was monitored following 6 or 25 min of perfusion. Of all cell lines tested, S364A L-selectin–GFP and CaM-RFP showed the highest FRET at both time points (Fig. 5 *A* and *B*). Moreover, FRET efficiency remained significantly higher in the transmigrated pseudopod at 25 min, suggesting that L-selectin S364 phosphorylation disrupts CaM binding specifically within transmigrating

pseudopods. In support of this conclusion, expression of L-selectin S364D had significantly lower FRET efficiency profiles at both time points in both transmigrated and nontransmigrated regions of the cell (Fig. 5 *A* and *B*).

Interestingly, FRET between CaM-RFP and S367A L-selectin–GFP was significantly lower than in WT in the transmigrated part of the cell at 6 min. This finding may have relevance to a recently reported role for phosphatidylserine in mediating interaction between the tail of L-selectin and the inner leaflet of the plasma membrane, preventing access for CaM binding (29). Note that at 6 and 25 min, FRET efficiency profiles of the S367D cell line were indistinguishable from FRET efficiency profiles of WT (Fig. 5 *A* and *B*). The significance of these findings is discussed later. In conclusion, these data provide strong evidence that the CaM/L-selectin interaction is negatively regulated by phosphorylation of S364.

Blocking L-Selectin Shedding Increases Monocyte Invasion Across Endothelial Cell Monolayers and Profoundly Alters Cell Polarity. To understand the biological significance of polarized L-selectin shedding better, monocyte transmigration behavior was closely monitored during perfusion experiments. Time-lapse movies of THP-1 cells expressing GFP alone, WT L-selectin–GFP, or ΔM-N L-selectin–GFP were compared on the basis of their protrusive behavior during TEM (Movies S4–S6). To quantify these observations, cells undergoing TEM were scored as having one, two, or multiple protrusions over early (6 min) and later (15 min) time points of continuous perfusion (Fig. S5). Expression of WT L-selectin–GFP, but not GFP alone, led to a significant increase in the overall number of cells pushing pseudopods beneath the endothelium at 6 min (Fig. 6*A* and Fig. S6*A*). This observation suggests that during early phases of TEM, L-selectin
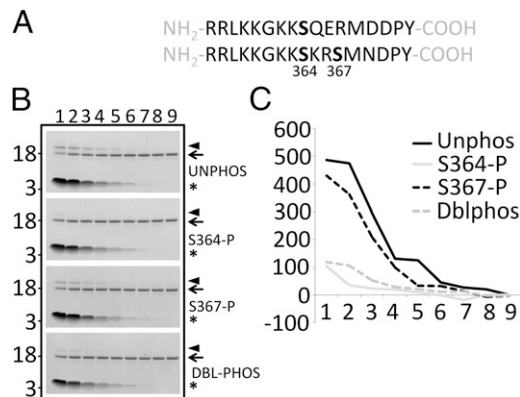

Fig. 4. Phosphorylation of L-selectin on Ser 364 blocks binding to CaM in vitro. (*A*) Amino acid sequence of the L-selectin cytoplasmic tail in the mouse (*Upper*) and human (*Lower*). Note that human L-selectin contains two Sers at positions 364 and 367. (*B*) Each lane (lanes 1–9) represents a single disuccinimidyl suberate (DSS) cross-linking experiment, resolved on a 4–12% Bis-Tris polyacrylamide gradient gel and subsequently stained with colloidal Coomassie. Decreasing concentrations of phosphorylated or nonphosphorylated L-selectin tail peptides (220, 110, 55, 27.50, 13.75, 6.88, 3.44, 1.72, and 0 μM) were incubated with 4.6 μM CaM for every cross-linking experiment. All cross-linking reactions contained 0.1 mM DSS. Asterisks denote the position of L-selectin peptide. Arrows denote the position of 4.6 μM recombinant CaM. Arrowheads denote the position of a 1:1 complex of CaM and L-selectin tail peptide. Molecular mass markers (3 and 18 kDa) are located to the left of every polyacrylamide gel. (*C*) Densitometric profile of each 1:1 cross-linked L-selectin/CaM complex (arrowhead in *B*). Densitometric readings (arbitrary units, *y* axis) are shown proceeding from the leftmost lane to the rightmost lane. The *x* axis is the lane number (lanes 1–9). All gels were scanned with a Li-COR quantitative IR imaging system and quantified using Image Studio 4.0 software. DBL-PHOS or Dblphos, double phosphorylated peptide; UNPHOS or Unphos, nonphosphorylated peptide.
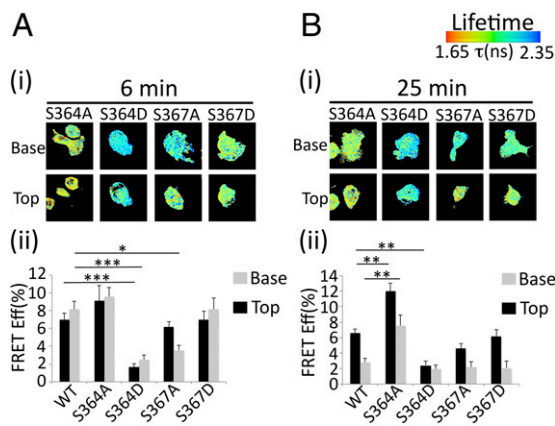
Fig. 5. S364 regulates binding to CaM in intact monocytes. THP-1 cells coexpressing CaM-RFP and WT or mutant L-selectin–GFP were perfused over TNF-activated HUVECs for 6 (*A*) or 25 (*B*) min, fixed in 4% (vol/vol) PFA, and prepared for FRET/FLIM analysis. All 25-min flow assays were perfused with THP-1 cells for the first 6 min, followed by 19 min of flow with media alone. This method ensured that every cell analyzed represented a minimum of 15 min of perfusion. (*i*) Representative lifetime images of transmigrating THP-1 cells coexpressing mutant L-selectin–GFP and CaM-RFP. Optical sections were taken above and below the endothelial monolayer. (*ii*) Analysis performed on at least 15 cells for each time point. A two-tailed unpaired Student's *t* test was used to calculate the difference in FRET efficiency (expressed as percentage, *y* axis) between Top and Base, and error bars represent SEM. *$P \leq 0.05$; **$P < 0.01$; ***$P < 0.001$. Lifetime is expressed as a pseudocolor scale from red (low lifetime with a very high probability of interaction) to blue (high lifetime with a very low probability of interaction).

potentiates invasive behavior in monocytes. By 15 min, the number of pseudopod extensions normalized between WT and GFP-alone cell lines, suggesting that L-selectin shedding at this time point may serve to limit the extent to which monocytes extend pseudopods beneath the endothelium.

Preincubating THP-1 cells expressing WT L-selectin–GFP with 10 μM TAPI-0 (WT + i, where i = inhibitor) led to significantly more cells presenting multiple protrusions (Fig. 6*B*), confirming that shedding was involved in curbing the protrusive behavior of transmigrating cells. In addition, significantly more multiple protrusions were also observed in ΔM-N mutant cells at 15 min (Fig. 6*B*). Control experiments confirmed that treatment with 10 μM TAPI-0 did not promote the formation of multiple protrusions in transmigrating THP-1 cells expressing GFP alone (Fig. S6 *C and D*), implying a specific effect of the inhibitor on blocking L-selectin shedding (Fig. 6*C*). Measurement of the subendothelial pseudopod area revealed significant increases in spread cell area, specifically where L-selectin shedding is genetically or pharmacologically blocked (Fig. 6*C*), correlating well with the invasive potential of L-selectin during TEM.

Although blocking L-selectin shedding with TAPI-0 in primary monocytes did not alter TEM rate or migration speed, a profound effect on cell shape and polarity was noted (Movie S7). Following TEM, primary monocytes presented with multiple protrusions, which was reminiscent of the phenotype presented by transmigrating THP-1 cells. To quantify these dynamic changes, cell outlines were captured frame by frame across a 25-min period of perfusion (*Materials and Methods*). The mean cell area of transmigrated monocytes was calculated per frame of every flow assay (Fig. 6*D* and Movies S8 and S9). Monocytes treated with DMSO had significantly larger mean cell areas than TAPI-0–treated cells. In contrast, TAPI-0–treated cells had longer cell perimeters and greater "longest axes," suggesting that despite their smaller cell area, they were more irregularly shaped (Fig. 6 *E* and *F*). This observation was further confirmed by assessment of their "shape factor," which defines the roundedness of cells, where

TAPI-0–treated monocytes were less round than DMSO controls (Fig. 6*G*). Confocal microscopic imaging also confirmed dramatic alteration in cell shape, using specimens that had been fixed and stained following 25 min of perfusion (Fig. S6*E*).

To quantify differences in monocyte protrusive behavior, the mean protrusion and retraction areas were calculated from each individual monocyte across three independent flow experiments and values were expressed as a percentage of the total cell area. DMSO-treated cells had significantly larger protrusion and retraction areas compared with TAPI-0–treated cells (Fig. 6*H*). This finding would imply the protrusions generated by TAPI-0–treated cells were inherently unstable, which was evident in the time-lapse movie provided in Movie S7. Fig. S6*E* further supports differences in cell shape between groups. Protrusion/retraction behavior was further quantified over time for three independent flow assays. By normalizing the net protrusion/retraction behavior to zero, it was possible to calculate the extent to which DMSO or TAPI-0–treated cells deviated from the zero line over time (Fig. 6*I*). A significant difference in the mean of the residuals was calculated between the two groups, suggesting greater erratic protrusion/retraction behavior in TAPI-0–treated cells as the flow assay progressed (Fig. 6*I*). Tracking the cell migratory behavior of transmigrated monocytes revealed DMSO-treated cells had significantly higher persistence in migration compared with TAPI-0–treated cells (Fig. 6*J*). These data further demonstrate the impact on migratory behavior as a consequence of disrupted cell polarity.

To exclude any possibility of the inhibitor promoting indirect effects on cell polarity, THP-1 cells expressing WT or ΔM-N L-selectin–GFP were challenged directly with 200 nM CCL2 chemokine (or monocyte chemoattractant protein-1, MCP-1) in micropipette assays (details are provided in *SI Materials and Methods*). A significantly higher proportion of THP-1 cells expressing WT L-selectin–GFP polarized toward the micropipette needle compared with ΔM-N cells (Fig. 6*K* and compare Movies S10 and S11). FACS analysis and Western blotting revealed that these responses were not due to aberrant CCR2 expression between cell lines (Fig. S7). Taken together, the data strongly suggest that blocking shedding of L-selectin has a profound impact on monocyte polarity, even under conditions that do not involve ligand binding of L-selectin.

Discussion

We have used a range of biochemical, cell biological, and advanced imaging approaches to demonstrate that shedding of L-selectin in human monocytes occurs precisely during TEM, and not before. This narrow window of opportunity for polarized L-selectin shedding appears to be critical in regulating monocyte invasion and polarity posttransmigration. As adherent leukocytes occupy valuable space on the inflamed endothelium, they become increasingly involved in actively recruiting bystander leukocytes from flow via leukocyte/leukocyte interaction (30, 31). This interaction behavior is known as secondary tethering and rolling, which has been observed during acute and chronic inflammatory responses (32, 33). Because the L-selectin/P-selectin glycoprotein ligand-1 pairing is critical in mediating these events, premature shedding of L-selectin during firm adhesion (or in the nontransmigrated part of the cell) would be detrimental to mechanisms that have evolved to amplify recruitment.

This study affirms L-selectin expression in monocytes is regulated differently between mice and humans. A recent study revealed that L-selectin expression is retained on murine monocytes that have emigrated from blood to the inflamed peritoneum (34). In contrast, an in vivo human study showed that monocytes lack L-selectin expression following migration into skin blisters (35). Although the methods used in each study cannot be compared directly, these findings do highlight possible differences that can exist between mouse and human systems. Because our in vitro model lacks the presence of basement membrane, pericytes, and
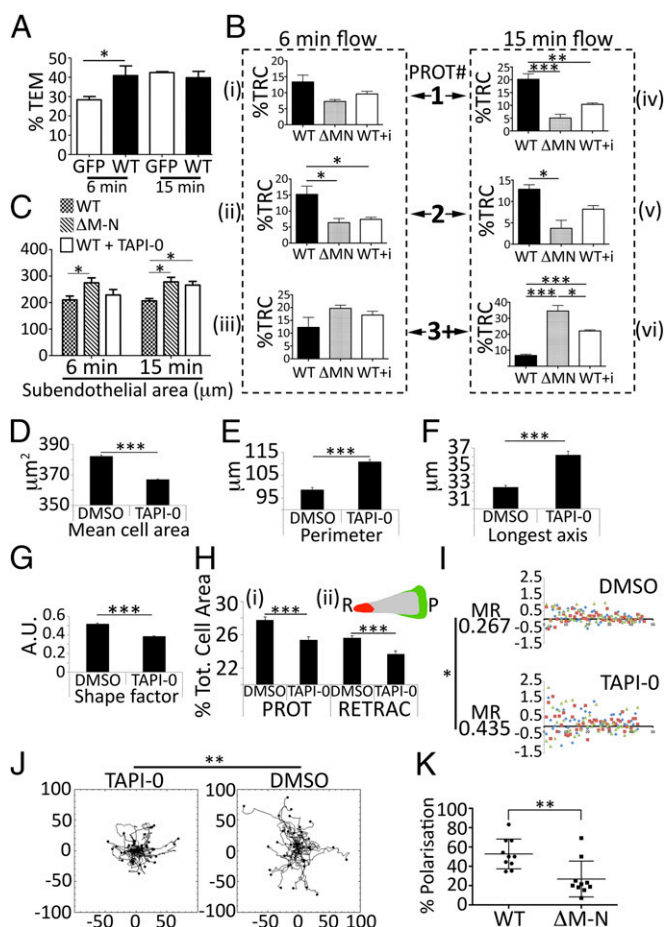
Fig. 6. Pharmacological or genetic blockade of L-selectin shedding has a dramatic impact on monocyte polarity. (A) Percentage of transmigrating THP-1 cells expressing WT L-selectin–GFP (WT) or GFP alone (GFP). Cells were monitored at 6 min or 15 min of continuous perfusion, and cells pushing protrusions beneath the endothelial monolayer were scored as a percentage of the total number bound at the end of every flow assay. Fig. S5 A and B provides a further breakdown of the types of protrusions that were scored (one, two, or multiple protrusions). The remaining cells adhered to the endothelium with no visible subendothelial protrusions. Data represent mean ± SEM. A two-tailed, unpaired Student's *t* test was used for statistical analysis. *$P < 0.05$. (B) Protrusion (PROT) dynamics scored between THP-1 cells expressing ΔM-N L-selectin, or WT L-selectin cells pretreated without or with 10 μM TAPI-0 (indicated as "WT + i" where i = inhibitor in bar graph). Cells forming one, two, or multiple protrusions (1, 2, or 3+) were scored (i–iii) after 6 min of flow or (iv–vi) after 15 min of flow. Data were expressed as percentage of total recruited cells (%TRC) at the end of the flow assay and represent mean ± SEM. A two-tailed, unpaired Student's *t* test was used for statistical analysis. *$P < 0.05$; **$P < 0.01$; ***$P < 0.001$. Fig. S5 C and D reveals that treatment of THP-1 cells expressing GFP alone with 10 μM TAPI-0 has no effect of protrusion dynamics at 6 or 15 min. (C) Spread area of all subendothelial pseudopods was measured using Volocity software and compared against WT, ΔM-N, and WT + 10 μm TAPI-0 cell lines. A two-tailed, unpaired Student's *t* test was used for statistical analysis. *$P < 0.05$. (D) Primary monocytes were perfused over TNF-activated HUVECs for a period of 10 min, followed by continuous perfusion of media for an additional 15 min. Mean cell areas were calculated for each group over three flow assays. The data represent more than 7,000 cells analyzed for each treatment. ***$P < 0.001$. (E–G) Volocity software was used to calculate the perimeter length, longest axis, and shape factor of nontouching cells during the flow assay. Data represent mean ± SEM. A two-tailed, unpaired Student's *t* test was used for statistical analysis. ***$P < 0.001$. (H) Using a bespoke Mathematica script (*Materials and Methods*), it was possible to measure the protrusion and retraction area of every transmigrated monocyte accurately. Dividing the protrusion or retraction area by the mean cell area (given in graph in D) provided a percentage of the total (Tot.) cell area dedicated to a protrusion or retraction, which is given in (i). Data were acquired from three independent flow assays and calculated for over 7,000

tissue resident macrophages, we cannot formally address the effect of L-selectin on monocyte polarity directly in humans. However, recent studies in mice have highlighted the involvement of such cell types and matrix components in directing the movement of posttransmigrated leukocytes to injured or infected cells and tissues (36–38).

We show that failure to shed L-selectin during TEM has a profound influence on front/back polarity and directional migration persistence. Venturi et al. (39) used an in vivo chemotaxis model to demonstrate that neutrophils expressing a sheddase-resistant form of L-selectin fail to emigrate far from their exit point compared with WT counterparts (39). Unlike the present study, the resolution of imaging achieved by Venturi et al. (39) was limited; thus, changes in cell morphology or the timing of L-selectin shedding could not be addressed. Our data may also help to explain why knocking out ADAM17 in vivo increases neutrophil recruitment to a site of bacterial infection (40), although its failure to resolve the infection better than WT neutrophils could be due to defective migration as a consequence of retained L-selectin expression in these cells. In support of our observations in monocytes, a previous study showed that pretreatment with a related sheddase inhibitor, RO 31-9790, at a dose of 30 μM resulted in normal neutrophil adhesion and transmigration rates under flow conditions (41). It is possible that these transmigrated neutrophils may phenocopy our observations, despite displaying normal transmigratory behavior. Interestingly, preincubating primary human monocytes with 50 μM GM6001 profoundly decreases the rate of TEM (42), which differs from our observations (Movie S7) and the aforementioned study with neutrophils (41). This discrepancy may be due to an excess of GM6001 used in the study. Understanding if our observation is unique to monocytes or common to other leukocyte subsets will be an important focus for future studies.

Our data show that WT L-selectin in transmigrating THP-1 cells preferentially clusters below the endothelial monolayer (Fig. 2D). Clustering of L-selectin could lead to two distinct but interrelated self-limiting events: phosphorylation of S364 (perhaps via activation of protein kinase C) and activation of ADAM17 (possibly via activation of p38 MAPK and phosphorylation of the ADAM17 cytoplasmic tail) (14). Numerous reports have shown that chondroitin, dermatan, and HSPG decorating the backbone of ECM proteins are credible ligands for L-selectin. These ligands include versican, biglycan, and collagen XVIII (23–26). In this report, we verify that biglycan is expressed in HUVECs and is sufficient to support the clustering of WT, but

cells. (ii) Color-coded cell represents a monocyte protrusion (P) in green and a retraction (R) in red (Movies S8 and S9 of DMSO and TAPI-0–treated cells, respectively). ***$P < 0.001$. (I) For every frame of every flow assay, it was possible to divide the mean protrusion area by the mean retraction area. Protrusion/retraction ratios that carried a value of 1 were normalized to 0, meaning any point carrying a positive value carried a net protrusion activity and any point with a negative value carried a net retraction activity. The x axis represents time expressed in frames over the 25-min period of flow. A Mann–Whitney statistical test (based on nonnormal variance), applied to the mean of the residual (MR) values calculated for the DMSO and TAPI-0 groups, reveals significantly higher variance in the TAPI-0 group (*$P = 0.011$). Orange squares, blue diamonds, and green triangles represent data points from three independent flow assays. (J) Following complete TEM, primary human monocytes were manually tracked and plotted onto circular histograms. All tracks (25 for each group) were positioned on a similar point of origin for comparison. **$P < 0.01$, Mann–Whitney test. The migration speed did not change between groups (DMSO = 7.6 ± 0.5 μm·min⁻¹, TAPI-0 = 6.4 ± 0.4 μm·min⁻¹). **$P = 0.10$, Mann–Whitney test. (K) THP-1 monocytes expressing WT or ΔM-N L-selectin were challenged with 200 nM CCL2 using a micropipette (Movies S10 and S11). Percentage polarization was scored according to the cells elongating and forming an extended lamellipodium toward the chemoattractant source. **$P < 0.01$, Mann–Whitney test. A total of 173 WT cells and 132 ΔM-N cells were analyzed over 10 separate experiments (total) on three separate days.

not ΔM-N, L-selectin (Fig. 2). Ligand density is known to act as a potent driver of shedding (43–45), and an increasing gradient of HSPG-like ligands across postcapillary venules could therefore influence L-selectin shedding. Also, a lack of shear stress in the subendothelial space could dramatically influence L-selectin clustering and subsequent signaling events that could feedback to activate ADAM17 locally and drive the shedding response specifically in pseudopods. The C-type lectin domain of the selectins has recently been shown to possess two potentially exclusive sites for binding sLe^x and HSPG (46). Systematic mutagenesis of these regions may identify the predicted HSPG-binding domain on L-selectin as the region responsible for clustering and shedding during TEM.

This report has increased our understanding of how CaM contributes to the shedding response during TEM, and also raises interesting new questions. It is clear from our work that phosphorylation at the conserved S364 site on L-selectin negatively regulates binding of CaM. Additionally, phosphorylation of the nonconserved S367 may be important in regulating the binding of the human L-selectin tail with the inner leaflet of the plasma membrane. An elegant in vitro study (29) recently showed that the inherently negatively charged phosphatidylserine, which resides specifically within the inner leaflet of the plasma membrane, interacts with the highly basic L-selectin tail, and consequently restricts CaM/L-selectin interaction. We found that FRET between S367A L-selectin–GFP and CaM-RFP was significantly lower compared with WT L-selectin–GFP following 6 min of perfusion (Fig. 5A). We reason that a sustained interaction between S367A and the phosphatidylserine-rich inner leaflet would prevent CaM binding. In contrast, FRET efficiency profiles between WT and S367D L-selectin were identical above and below the endothelium, and across both time points (Fig. 5). This finding would suggest that phosphorylation of L-selectin at S367 is required to "peel" the tail off from the inner leaflet of the plasma membrane and that S364 phosphorylation is required to block CaM binding. Previous work from Kilian et al. (28) reveals a role for different protein kinase C isozymes in phosphorylating these sites; thus, understanding how this phosphorylation is regulated during TEM would be highly relevant for future study.

TEM is a form of cell invasion, and immune cells are often compared with cancer cells in this regard. It is likely that retention of L-selectin expression during the very early phases of transmigration is required for invasive-type behavior in monocytes. We observed a consistent increase in pseudopod number in THP-1 cells expressing WT L-selectin–GFP at early time points, which decreased as shedding ensued (Fig. 6B). Although L-selectin is abundantly expressed on most circulating leukocytes, it is not restricted to this cell type. L-selectin is expressed in human trophoblasts, and its role is thought to promote tethering of developing embryos to the underlying endometrium (47). In addition, it has been postulated that L-selectin may localize to the leading edge of trophoblasts to facilitate attachment to the maternal vasculature as trophoblasts invade the endometrium and chemotax toward their target vessels (48). This hypothetical view would further support the notion that L-selectin is a proinvasion molecule and that its shedding is required to fine-tune the extent of its participation in invasion during specific cellular events. ERM are known binding partners of L-selectin, are thought to regulate adhesion and shedding, and can act both upstream and downstream of Rho-GTPase activation (49). It is therefore possible that L-selectin/ERM binding is required for driving multiple protrusions, as seen in the ΔM-N L-selectin–expressing cells. Continued L-selectin/ERM interaction within subendothelial pseudopods could result in localized activation of Rho-GTPases, leading to localized integrin-dependent adhesion, actin polymerization, and membrane protrusion. Using L-selectin mutants that abrogate interaction with ERM will allow exploration of this mechanism in future studies.

Materials and Methods

Antibodies and Reagents. Unless otherwise stated, all reagents were purchased from Sigma–Aldrich. Generation of the anti-human L-selectin monoclonal antibody (IgG1) LAM1-14 is described in a previous report (16). The anti-mouse L-selectin monoclonal antibody (IgG1) MEL-14 was purchased from Santa Cruz Biotechnology. Biotinylated sLe^x was purchased from Glycotech, and NeutrAvidin was purchased from Pierce. Antivinculin mouse monoclonal antibody was purchased from Sigma–Aldrich. Rabbit antibiglycan and anti-CCR2 antibodies were purchased from Abcam. All Alexa Fluor secondary antibodies were purchased from Life Technologies. Recombinant purified biglycan was purchased from R&D Systems.

Cell Lines. All cell lines were cultured at 37 °C, containing 5% CO$_2$ in a humidified atmosphere. Details of how they were propagated can be found in *SI Materials and Methods*.

Molecular Biology and Biochemistry. These techniques are detailed in *SI Materials and Methods*.

FRET/FLIM Analysis. FLIM measurement of FRET was performed with a multiphoton microscope system as described previously. A Nikon TE2000E inverted microscope, combined with an in-house scanner and Chameleon Ti:Sapphire ultrafast pulsed multiphoton laser (Coherent, Inc.), was used for excitation of GFP (at 890 nm). Fluorescence lifetime imaging capability was provided by time-correlated, single-photon counting electronics (SPC 700; Becker & Hickl). A 40× objective (N.A. = 1.3) was used throughout, and data were acquired at 500 ± 20 nm through a bandpass filter (35-5040; Coherent, Inc.). Acquisition times on the order of 300 s at low excitation power were used to achieve sufficient photon statistics for fitting, avoiding either pulse pile-up or significant photobleaching. Data were analyzed as previously described (50, 51). The FRET efficiency is related to the molecular separation of donor and acceptor and the fluorescence lifetime of the interacting fraction by

$$\eta FRET = (R06/(R06 + r6)) = 1 - \tau FRET \ \tau d,$$

where ηFRET is the FRET efficiency, R0 is the Förster radius, r is the molecular separation, τFRET is the lifetime of the interacting fraction, and τd is the lifetime of the donor in the absence of an acceptor. The donor-only control is used as the reference against which all of other lifetimes are calculated in each experiment. τFRET and τd can also be taken to be the lifetime of the interacting fraction and noninteracting fraction, respectively. Quantification of FRET was made from all pixels within each cell that was analyzed. All image collection and data analysis were performed using TRI2 software (developed by Paul Barber, Gray Cancer Institute, London, United Kingdom).

Parallel Plate Flow Chamber Assays. All flow experiments were performed using a flow chamber 35 mm in diameter that was engineered by Glycotech. All perfusion experiments were performed at 1.5 dyn/cm^2 using a Harvard Apparatus 2000 PHD syringe pump. Perfusion media consisted of RPMI supplemented with L-glutamine, 10% FCS, 1% penicillin/streptomycin, 50 μM β-mercaptoethanol, and 25 mM Hepes. HUVECs were seeded onto glass coverslips 35 mm in diameter (no. 1 thickness; VWR) precoated with 10 μg·mL^{-1} fibronectin. Before each perfusion assay, HUVECs were stimulated overnight (16 h) with 10 ng·mL^{-1} carrier-free recombinant human TNF-α (R&D Systems). Each perfusion assay was performed under times specified in *Results*. THP-1 cells were perfused at a density of 0.5 × 10^6 cells per milliliter, and primary monocytes were perfused at a density of 1 × 10^6 cells per milliliter. Monocytes treated with 10 μM TAPI-0 required a preincubation time of 10 min at 37 °C before perfusion over TNF-activated HUVECs. Note that the perfusate would also contain 10 μM TAPI-0. Note that in Fig. S6 *C and D*, TAPI-0 did not alter protrusive behavior in THP-1 cells lacking L-selectin.

Coperfusion experiments performed in Figs. S2F and S6E (for labeling primary monocytes) were used to monitor recruitment between two different cell lines. Cells were preloaded with 1 μM Cell Tracker Green or Orange (both from Molecular Probes, Life Technologies) for 10 min in neat RPMI containing 25 mM Hepes for 10 min at 37 °C. Labeled cells were harvested by centrifugation and mixed in equal quantities. Mixed cell populations were counted under green and red fluorescence channels to verify that they were indeed mixed to 1:1 ratios. Any deviations from this ratio were noted and used to normalize the total number of cells scored in coperfusion assays. Cell Tracker dyes were swapped periodically between cell lines, and between experiments, to ensure the dyes did not have any adverse effect on recruitment per se.

For confocal analysis, coverslips were detached from the flow chamber at the end of each flow assay and immediately submerged in 4% (vol/vol) PFA

solution for 10–15 min at room temperature. Cells were washed four to five times in PBS to remove excess PFA and permeabilized for 3 min in ice-cold PBS containing 0.1% (vol/vol) Nonidet P-40 substitute (Fluka). After gently washing off the permeabilization buffer, coverslips were blocked in 10% FCS containing FcR block (Miltenyi Biotec Ltd.) overnight at 4 °C. Specimens were then labeled with appropriate primary and secondary antibodies and relevant dilutions (diluted in similar block solution). Note that a PBS wash, followed by a blocking step, was included between primary and secondary antibody staining. Coverslips were finally washed four to five times in PBS and mounted onto glass slides using fluorescence mounting medium (Dako).

The rolling assays shown in Fig. S2E were performed as previously published (52). In brief, NeutrAvidin was immobilized onto the bottom of six-well dishes and blocked using 5% (vol/vol) BSA in PBS. Biotinylated sLe^x was added in excess to each well at a concentration of 1 μg·mL^{-1}.

Image stacks from phase contrast channels of time-lapse movies were imported into Wolfram Mathematica 10 for processing and analysis. Images were thresholded using the in-built command "LocalAdaptiveBinarize." Thresholded image stacks were then partitioned into overlapping pairs and combined into an RGB (Red–Green–Blue) color image using a third blank image for the blue channel. Overlapping objects in these RGB images consisted of red pixels, green pixels, and yellow pixels. Red pixels correspond to objects that were present in the first image, but not in the second, and to regions of retraction. The green pixels correspond to objects present in the second image, but not in the first, and to regions of protrusion. Yellow corresponded to objects present in both images. Yellow pixels were converted to gray so that regions of overlap could be differentiated more easily from protruding and retracting regions. Because some of the objects present in these protrusion/retraction maps were either large endothelial cells that had shifted slightly or much smaller monocytes that had not yet transmigrated, a selection protocol was devised to remove unwanted objects. To be selected, objects had to have red and green pixels to suggest active protrusion/retraction; there also there had to be an area of overlap, but that overlap was restricted to less than 90%. Next, pixel counts for objects had to be larger than a defined value but less than double this size. Because monocytes were migrating appreciable distances in all observed cases, a final selection process was used to remove objects that had not moved more than a few pixels. Selected objects were then analyzed for the number of red, green, and gray pixels and exported for further analysis in Excel (Microsoft Corp.).

Tracking of Transmigrated Primary Monocytes. For analysis of cell speed and persistence, cells were manually tracked using ImageJ (NIH), and migratory parameters were calculated using a Mathematica notebook written and provided by G. A. Dunn and G. E. Jones, Kings College, London, United Kingdom. A more comprehensive documentation of how the analysis was undertaken can be found in a report by Ahmed et al. (53).

All other methods are described in SI Materials and Methods.

1. Muller WA (2014) How endothelial cells regulate transmigration of leukocytes in the inflammatory response. *Am J Pathol* 184(4):886–896.
2. Ley K, Laudanna C, Cybulsky MI, Nourshargh S (2007) Getting to the site of inflammation: The leukocyte adhesion cascade updated. *Nat Rev Immunol* 7(9):678–689.
3. Zarbock A, Ley K (2008) Mechanisms and consequences of neutrophil interaction with the endothelium. *Am J Pathol* 172(1):1–7.
4. Schmidt S, Moser M, Sperandio M (2013) The molecular basis of leukocyte recruitment and its deficiencies. *Mol Immunol* 55(1):49–58.
5. Herter J, Zarbock A (2013) Integrin Regulation during Leukocyte Recruitment. *J Immunol* 190(9):4451–4457.
6. Rullo J, et al. (2012) Actin polymerization stabilizes α4β1 integrin anchors that mediate monocyte adhesion. *J Cell Biol* 197(1):115–129.
7. Ivetic A (2013) Signals regulating L-selectin-dependent leucocyte adhesion and transmigration. *Int J Biochem Cell Biol* 45(3):550–555.
8. Arbonés ML, et al. (1994) Lymphocyte homing and leukocyte rolling and migration are impaired in L-selectin-deficient mice. *Immunity* 1(4):247–260.
9. Hickey MJ, et al. (2000) L-selectin facilitates emigration and extravascular locomotion of leukocytes during acute inflammatory responses in vivo. *J Immunol* 165(12):7164–7170.
10. Smalley DM, Ley K (2005) L-selectin: Mechanisms and physiological significance of ectodomain cleavage. *J Cell Mol Med* 9(2):255–266.
11. Peschon JJ, et al. (1998) An essential role for ectodomain shedding in mammalian development. *Science* 282(5392):1281–1284.
12. Kahn J, Walcheck B, Migaki GI, Jutila MA, Kishimoto TK (1998) Calmodulin regulates L-selectin adhesion molecule expression and function through a protease-dependent mechanism. *Cell* 92(6):809–818.
13. Ivetic A, et al. (2004) Mutagenesis of the ezrin-radixin-moesin binding domain of L-selectin tail affects shedding, microvillar positioning, and leukocyte tethering. *J Biol Chem* 279(32):33263–33272.
14. Killock DJ, Ivetić A (2010) The cytoplasmic domains of TNFalpha-converting enzyme (TACE/ADAM17) and L-selectin are regulated differently by p38 MAPK and PKC to promote ectodomain shedding. *Biochem J* 428(2):293–304.
15. Zhao L, Shey M, Farnsworth M, Dailey MO (2001) Regulation of membrane metalloproteolytic cleavage of L-selectin (CD62l) by the epidermal growth factor domain. *J Biol Chem* 276(33):30631–30640.
16. Spertini O, Kansas GS, Reimann KA, Mackay CR, Tedder TF (1991) Function and evolutionary conservation of distinct epitopes on the leukocyte adhesion molecule-1 (TQ-1, Leu-8) that regulate leukocyte migration. *J Immunol* 147(3):942–949.
17. Bruehl RE, Springer TA, Bainton DF (1996) Quantitation of L-selectin distribution on human leukocyte microvilli by immunogold labeling and electron microscopy. *J Histochem Cytochem* 44(8):835–844.
18. Killock DJ, et al. (2009) In Vitro and in Vivo Characterization of Molecular Interactions between Calmodulin, Ezrin/Radixin/Moesin, and L-selectin. *J Biol Chem* 284(13):8833–8845.
19. Ivetic A, Deka J, Ridley A, Ager A (2002) The cytoplasmic tail of L-selectin interacts with members of the Ezrin-Radixin-Moesin (ERM) family of proteins: Cell activation-dependent binding of Moesin but not Ezrin. *J Biol Chem* 277(3):2321–2329.
20. Luscinskas FW, et al. (1994) Monocyte rolling, arrest and spreading on IL-4-activated vascular endothelium under flow is mediated via sequential action of L-selectin, beta 1-integrins, and beta 2-integrins. *J Cell Biol* 125(6):1417–1427.
21. Zinchuk V, Zinchuk O, Okada T (2007) Quantitative colocalization analysis of multi-color confocal immunofluorescence microscopy images: Pushing pixels to explore biological phenomena. *Acta Histochem Cytochem* 40(4):101–111.
22. Migaki GI, Kahn J, Kishimoto TK (1995) Mutational analysis of the membrane-proximal cleavage site of L-selectin: Relaxed sequence specificity surrounding the cleavage site. *J Exp Med* 182(2):549–557.
23. Kawashima H, et al. (1999) Identification and characterization of ligands for L-selectin in the kidney. I. Versican, a large chondroitin sulfate proteoglycan, is a ligand for L-selectin. *Int Immunol* 11(3):393–405.
24. Kawashima H, et al. (2000) Binding of a large chondroitin sulfate/dermatan sulfate proteoglycan, versican, to L-selectin, P-selectin, and CD44. *J Biol Chem* 275(45):35448–35456.
25. Kitaya K, Yasuo T (2009) Dermatan sulfate proteoglycan biglycan as a potential selectin L/CD44 ligand involved in selective recruitment of peripheral blood CD16(-) natural killer cells into human endometrium. *J Leukoc Biol* 85(3):391–400.
26. Kawashima H, et al. (2003) Collagen XVIII, a basement membrane heparan sulfate proteoglycan, interacts with L-selectin and monocyte chemoattractant protein-1. *J Biol Chem* 278(15):13069–13076.
27. Stoler-Barak L, et al. (2014) Blood vessels pattern heparan sulfate gradients between their apical and basolateral aspects. *PLoS ONE* 9(1):e85699.
28. Kilian K, Dernedde J, Mueller EC, Bahr I, Tauber R (2004) The interaction of protein kinase C isozymes alpha, iota, and theta with the cytoplasmic domain of L-selectin is modulated by phosphorylation of the receptor. *J Biol Chem* 279(33):34472–34480.
29. Deng W, Srinivasan S, Zheng X, Putkey JA, Li R (2011) Interaction of calmodulin with L-selectin at the membrane interface: Implication on the regulation of L-selectin shedding. *J Mol Biol* 411(1):220–233.
30. Kolaczkowska E, Kubes P (2013) Neutrophil recruitment and function in health and inflammation. *Nat Rev Immunol* 13(3):159–175.
31. An G, et al. (2008) P-selectin glycoprotein ligand-1 is highly expressed on Ly-6Chi monocytes and a major determinant for Ly-6Chi monocyte recruitment to sites of atherosclerosis in mice. *Circulation* 117(25):3227–3237.
32. Eriksson EE, Xie X, Werr J, Thoren P, Lindbom L (2001) Importance of primary capture and L-selectin-dependent secondary capture in leukocyte accumulation in inflammation and atherosclerosis in vivo. *J Exp Med* 194(2):205–218.
33. Lim YC, et al. (1998) Important contributions of P-selectin glycoprotein ligand-1-mediated secondary capture to human monocyte adhesion to P-selectin, E-selectin, and TNF-alpha-activated endothelium under flow in vitro. *J Immunol* 161(5):2501–2508.
34. Tang J, et al. (2011) Adam17-dependent shedding limits early neutrophil influx but does not alter early monocyte recruitment to inflammatory sites. *Blood* 118(3):786–794.
35. Evans BJ, et al. (2006) Shedding of lymphocyte function-associated antigen (LFA-1) in a human inflammatory response. *Blood* 107(9):3593–3599.
36. Lämmermann T, et al. (2013) Neutrophil swarms require LTB4 and integrins at sites of cell death in vivo. *Nature* 498(7454):371–375.
37. Proebstl D, et al. (2012) Pericytes support neutrophil subendothelial cell crawling and breaching of venular walls in vivo. *J Exp Med* 209(6):1219–1234.
38. Stark K, et al. (2013) Capillary and arteriolar pericytes attract innate leukocytes exiting through venules and 'instruct' them with pattern-recognition and motility programs. *Nat Immunol* 14(1):41–51.
39. Venturi GM, et al. (2003) Leukocyte migration is regulated by L-selectin endoproteolytic release. *Immunity* 19(5):713–724.
40. Long C, Hosseinkhani MR, Wang Y, Sriramarao P, Walcheck B (2012) ADAM17 activation in circulating neutrophils following bacterial challenge impairs their recruitment. *J Leukoc Biol* 92(3):667–672.

41. Allport JR, et al. (1997) L-selectin shedding does not regulate human neutrophil attachment, rolling, or transmigration across human vascular endothelium in vitro. *J Immunol* 158(9):4365–4372.

42. Tsubota Y, Frey JM, Tai PW, Welikson RE, Raines EW (2013) Monocyte ADAM17 promotes diapedesis during transendothelial migration: Identification of steps and substrates targeted by metalloproteinases. *J Immunol* 190(8):4236–4244.

43. Liu S, Kiick K (2011) Architecture effects on L-selectin shedding induced by polypeptide-based multivalent ligands. *Polymer Chem* 2(7):1513–1522.

44. Gordon EJ, Strong LE, Kiessling LL (1998) Glycoprotein-inspired materials promote the proteolytic release of cell surface L-selectin. *Bioorg Med Chem* 6(8):1293–1299.

45. Mowery P, et al. (2004) Synthetic glycoprotein mimics inhibit L-selectin-mediated rolling and promote L-selectin shedding. *Chem Biol* 11(5):725–732.

46. Martinez P, et al. (2013) Over-sulfated glycosaminoglycans are alternative selectin ligands: Insights into molecular interactions and possible role in breast cancer metastasis. *Clin Exp Metastasis* 30(7):919–931.

47. Genbacev OD, et al. (2003) Trophoblast L-selectin-mediated adhesion at the maternal-fetal interface. *Science* 299(5605):405–408.

48. Fazleabas AT, Kim JJ (2003) Development. What makes an embryo stick? *Science* 299(5605):355–356.

49. Ivetic A, Ridley AJ (2004) Ezrin/radixin/moesin proteins and Rho GTPase signalling in leucocytes. *Immunology* 112(2):165–176.

50. Parsons M, Messent AJ, Humphries JD, Deakin NO, Humphries MJ (2008) Quantification of integrin receptor agonism by fluorescence lifetime imaging. *J Cell Sci* 121(Pt 3):265–271.

51. Parsons M, et al. (2005) Spatially distinct binding of Cdc42 to PAK1 and N-WASP in breast carcinoma cells. *Mol Cell Biol* 25(5):1680–1695.

52. Burns SO, et al. (2010) A congenital activating mutant of WASp causes altered plasma membrane topography and adhesion under flow in lymphocytes. *Blood* 115(26):5355–5365.

53. Ahmed T, Shea K, Masters JR, Jones GE, Wells CM (2008) A PAK4-LIMK1 pathway drives prostate cancer cell migration downstream of HGF. *Cell Signal* 20(7):1320–1328.